Astron. Astrophys. 341, 491–498 (1999)

ASTRONOMY AND ASTROPHYSICS

Keck observations of the black-hole candidate GRO J0422+32⋆

E. Harlaftis[1,⋆⋆], **S. Collier**[1], **K. Horne**[1], **and A.V. Filippenko**[2]

[1] School of Physics and Astronomy, University of St. Andrews, KY16 9SS, UK
(e-mail: ehh@astro.noa.gr; sjc2@st-and.ac.uk; kdh1@st-andrews.ac.uk)
[2] Department of Astronomy, University of California, Berkeley, CA 94720-3411, USA (e-mail: alex@astro.berkeley.edu)

Received 10 August 1998 / Accepted 21 October 1998

Abstract. Keck observations of the black-hole candidate GRO J0422+32 in quiescence have been used by Filippenko, Matheson, & Ho (1995) to determine a mass function $f(M_{\rm x}) = 1.21 \pm 0.06\ M_\odot$ for the compact object. Reanalysis of the data shows that the mass ratio, $q = M_{\rm c}/M_{\rm x}$, is $q = 0.116^{+0.079}_{-0.071}$ from the rotational broadening of the companion star $v \sin i = 90^{+22}_{-27}$ km s^{-1} (1σ). From q and the mass function (slightly revised to $1.13 \pm 0.09\ M_\odot$), we derive the mass of the compact object, $M_{\rm x} = (1.4 \pm 0.2)\ \sin^{-3} i\ M_\odot$. The companion star (M2$^{+2}_{-1}$ spectral type) contributes 61 ± 4% of the light at red wavelengths. An Hα Doppler image of the system shows the typical ring-like distribution of an accretion disk. Emissivity laws for Hα in black-hole binaries roughly follow an $R^{-1.5}$ law, which is also supported by GRO J0422+32. The Li I λ6708 absorption line is not detected (1σ equivalent width limit of 0.13 Å), in contrast to four other X-ray binaries.

Key words: black hole physics – stars: binaries: close – stars: individual: GRO J0422+32 – stars: novae, cataclysmic variables – X-rays: stars

1. Introduction

The past decade of studies of Galactic black-hole candidates has been marked by the effort to find a compact object unequivocably heavier than the maximum mass of a neutron star ($\sim 3.2\ M_\odot$; van Paradijs & McClintock 1995 and references therein). This was accomplished with the measurement of the mass functions of V404 Cyg [$f(M_{\rm x}) = 6.08 \pm 0.06\ M_\odot$; Casares, Charles, & Naylor 1991; Casares & Charles 1994] and GS 2000+25 [$f(M_{\rm x}) = 4.97 \pm 0.10\ M_\odot$; Filippenko, Matheson, & Barth 1995, hereafter FMB; Casares, Charles, & Marsh 1995]; these represent the minimum mass of the compact object in the binary system. Determination of the compact object mass is possible only by modeling the ellipsoidal modulations of the companion star in the infrared as a function of (q, i) and by measuring q directly from the rotational broadening of the companion star. There are few objects both methods have been attempted such as GS 2000+25 (see for the inclination Callanan et al. 1996a and Beekman et al. 1996, and for the mass ratio Harlaftis, Horne, & Filippenko 1996, hereafter HHF).

Dynamical evidence from observations of the X-ray nova GRO J0422+32 with the first of the W. M. Keck 10-m telescopes in Hawaii (Filippenko, Matheson, & Ho 1995; hereafter FMH) gives a mass function $f(M_{\rm x}) = 1.21 \pm 0.06\ M_\odot$ through the detection of the M-type companion star (semi-amplitude $K_{\rm c} = 380.6 \pm 6.5$ km s^{-1}), consistent with independent estimates by Casares et al. [1995a; $f(M_{\rm x}) = 0.85 \pm 0.30\ M_\odot$] and Orosz & Bailyn [1995; $f(M_{\rm x}) = 0.9 \pm 0.4\ M_\odot$]. The reader should refer to FMH for an overview of GRO J0422+32, a description of the Keck observations with the low resolution imaging spectrometer (LRIS; Oke et al. 1995), and the derivation of the mass function of the compact object. A total of 21 long-slit CCD spectra were obtained on four nights (1994 November 8, 9 and 1995 January 26, 27 UT; see Table 1 for a log of observations). Here, we perform an analysis similar to the one we undertook on GS 2000+25 (HHF) and Nova Ophiuchi 1977 (Harlaftis, Steeghs, Horne, Filippenko 1997, hereafter HSHF) to determine the rotational broadening of the companion star to GRO J0422+32 (which gives the system's mass ratio) and to investigate the Hα emission-line distribution.

2. Spectra and light curves

The average spectrum for each night of observation is shown in Fig. 1. Measurements of the nightly averages of the continuum flux density in the range 6600–6800 Å, the Hα emission-line flux integrated between –1900 and +1900 km s^{-1} of the line center, and the Hα equivalent width (EW) are given in Table 2. The continuum rises by 40% and the line flux by 50% within one day (January 26–27). The EW of Hα is a factor of 9 higher than in GS 2000+25 (HHF). Note the change in strength of the blue peak in the Hα profile between 1994 November and 1995 January. A similar profile was observed in GRO J0422+32 during its mini-outburst in 1993 December (Casares et al. 1995b) and during a fainter phase between the two mini-outbursts that occurred in August and November 1993 (see Fig. 2 in Garcia et al. 1996). An unusual Hα line profile has also been observed in

Send offprint requests to: E. Harlaftis

⋆ Based on observations obtained at the W.M. Keck Observatory

⋆⋆ *Present address:* Astronomical Institute, National Observatory of Athens, Lofos Nymfon, P.O. Box 20048, Athens 11810, Greece

Table 1. Journal of observations

No	Date	UT(mid)	Exp. (s)	HJD[a]	Phase[b]	V^{c}	V_R^{d}	Smear[e]
1	11/8/94	09:52:49	1800	9664.91684	16.47532	124.0 ± 19.6	69.5	224
2	11/8/94	11:07:49	1800	9664.96892	16.72146	-325.7 ± 19.0	-354	40
3	11/8/94	11:42:21	1800	9664.99291	16.83480	-195.8 ± 30.7	-308.4	116
4	11/8/94	12:37:40	1800	9665.03131	17.01628	-2.8 ± 31.0	50	225
5	11/8/94	13:08:38	1800	9665.05283	17.11796	245.7 ± 26.6	233.2	166
6	11/9/94	12:35:11	1800	9666.02964	21.73403	-367.0 ± 15.3	-358.1	22
7	11/9/94	13:11:25	1800	9666.05479	21.85289	-271.5 ± 15.9	-284.9	137
8	11/9/94	13:44:11	1800	9666.07754	21.96043	5.7 ± 21.7	-79.5	220
9	11/9/94	14:14:39	1800	9666.09871	22.06047	124.4 ± 24.0	150	210
10	1/26/95	05:54:29	1800	9743.74923	389.0115	70.7 ± 29.5	38.9	226
11	1/26/95	06:25:03	1800	9743.77046	389.1118	298.3 ± 22.1	252.3	172
12	1/26/95	06:55:33	1800	9743.79164	389.2119	388.7 ± 16.5	373.4	53
13	1/26/95	07:29:14	1800	9743.81503	389.3224	339.0 ± 15.1	346.2	100
14	1/26/95	07:59:47	1800	9743.83623	389.4226	134.6 ± 28.3	185.9	201
15	1/26/95	08:30:12	1800	9743.85736	389.5225	-179.4 ± 44.2	-40.4	224
16	1/26/95	09:06:31	2100	9743.88258	389.6417	-375.0 ± 31.3	-277.1	165
17	1/26/95	09:42:50	2200	9743.90780	389.7608	-351.3 ± 17.7	-359.1	20
18	1/26/95	10:24:10	2700	9743.93650	389.8965	-281.0 ± 18.9	-213.2	265
19	1/27/95	05:49:17	1800	9744.74554	393.7197	-306.2 ± 13.5	-353.3	42
20	1/27/95	06:19:45	1800	9744.76670	393.8197	-389.5 ± 11.1	-324.9	97
21	1/27/95	06:52:49	1800	9744.78966	393.9282	-116.0 ± 21.7	-150.2	204

[a] HJD–2,440,000 at midpoint of exposure.
[b] Using $P = 0.21161$ d and $T_0 = 2,449,661.4305$.
[c] Radial velocities (km s^{-1}) extracted using the M2 template.
[d] Radial velocities (km s^{-1}) from orbital solution using the M2 template.
[e] Orbital broadening (km s^{-1}) using the M2 V radial-velocity curve for the phases observed.

Table 2. Average properties

Date	No	HJD[a]	F_ν^{b}	Flux(Hα)[c]	EW(Hα)[d]
11/8/94	5	9664.97	0.0215	3.22	204
11/9/94	4	9666.06	0.0221	3.44	214
1/26/95	9	9743.83	0.0187	2.53	181
1/27/95	3	9744.77	0.0264	3.76	189

[a] HJD–2,440,000 at midpoint of night.
[b] Continuum flux density in the range 6600–6800 Å (mJy; the uncertainty is 1 in the last digit).
[c] Hα emission-line flux (10^{-15} erg s^{-1} cm^{-2}; the uncertainty is 2 in the last digit).
[d] Equivalent width of Hα emission (Å; the uncertainty is 1 Å).

Nova Oph 1977 during quiescence (see Fig. 2 in Remillard et al. 1996).

The orbital light curves for the continuum and Hα are illustrated in Fig. 2 (full orbital coverage was obtained only on January 26). The continuum shows ellipsoidal variations (maxima at quadrature phases 0.25, 0.75 and minima at conjunction phases 0.0, 0.5). A sinusoidal plus constant fit gives a 4% variation over the constant of 0.0187 ± 0.0001 mJy (6600–6800 Å), which is consistent with the ~ 0.1 mag ellipsoidal variations in the I-band reported by Casares et al. (1995a). The peak at phase 0.25 is slightly stronger than the peak at phase 0.75; the asymmetry in the maxima may suggest contamination from the accretion disk. Haswell (1995) proposed that such asymmetries in the maxima of the ellipsoidal variation in A0620–00 may arise due to a non-circular disk which precesses on a timescale much longer than the orbital period.

The Hα light curve in Fig. 2(b) shows a sinusoidal variation peaking at phase ~ 0.30; this phase is not associated with the companion star or the bright spot, but it can be related to the larger hump of the ellipsoidal variation. A model using a constant and a sine function gives $(2.37 \pm 0.01) \times 10^{-15}$ ergs cm^{-2} s^{-1} for the constant and $(0.15 \pm 0.02) \times 10^{-15}$ ergs cm^{-2} s^{-1} for the semi-amplitude of the sine (6%). It is interesting to note that the radial velocity curve of Hα has a *leading* phase shift of 0.3 with respect to the companion star (FMH), and a sinusoidal flux variation on 1995 January 26 which peaks at orbital phase 0.3. The former phase shift can be explained assuming line emission from the gas stream (see, for example, Welsh et al. 1995). An extended outer rim on the disk at around phase 0.8, which is blocking the inner-disk light at that phase but revealing its irradiated inner side at phase 0.3, may then be required to interpret the Hα flux variation.

3. Radial velocities revisited

We checked FMH's results by reducing the 21 spectra using a different software package (a data reduction package called PAMELA (Horne 1986) instead of FMH's use of own and IRAF software) and by performing the radial velocity anal-

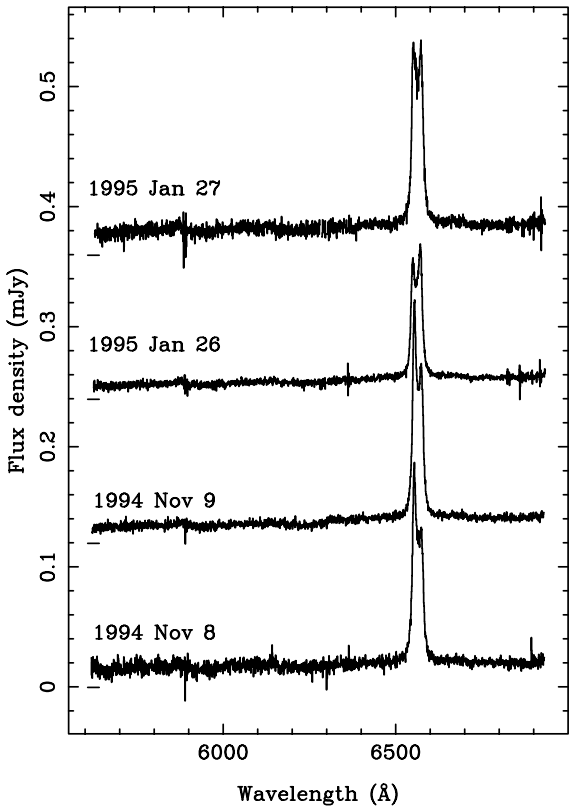

Fig. 1. Average spectra of GRO J0422+32 obtained with the W. M. Keck telescope on 1994 November 8 and 9, and on 1995 January 26 and 27 UT. Successive offsets of 0.12 mJy have been used for clarity. Dashes denote the zero continuum level. Note the stronger blue part of the Hα profile in November.

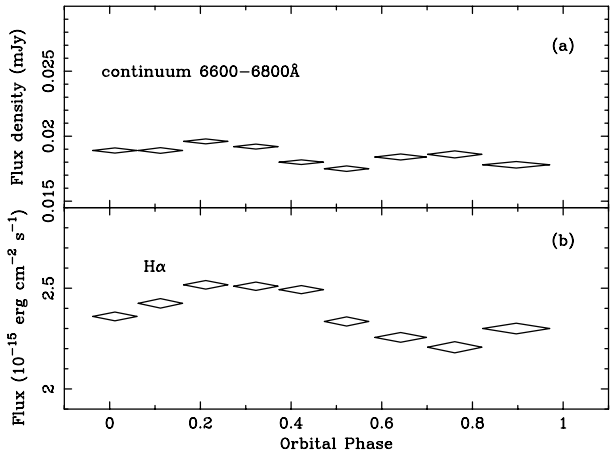

Fig. 2a and b. Light curves of **a** the continuum and **b** the Hα emission line of GRO J0422+32 on 1995 January 26; the abscissa is the orbital phase. The Hα curve shows a sinusoidal variation, in contrast to the ellipsoidal variation of the continuum.

ysis anew. To improve the signal-to-noise (S/N) ratio over that obtained by FMH, the spectra were optimally extracted (Horne 1986); statistical uncertainties were also produced during the extraction stage. The detailed procedure is very similar to that presented in HHF. The results are shown in Table 3 and the salient points follow. For the M-type template stars, we find $365 < K_{\rm c} < 372\,{\rm km\,s^{-1}}$ and a weighted average of $\gamma = 9 \pm 8\,{\rm km\,s^{-1}}$. Casares et al. (1995a) classified the companion as an M2 $\pm$ 2 V star from the TiO bands, and FMH similarly found an M2 spectral type. We adopt the M2 spectral type for the radial-velocity ephemeris

$$V_R = \gamma + K_{\rm c}\,\left[\sin\frac{2\,\pi}{P}(t - T_0)\right],$$

with $\gamma = 11 \pm 8\,{\rm km\,s^{-1}}$, $K_{\rm c} = 372 \pm 10\,{\rm km\,s^{-1}}$, $T_0(HJD) = 2,449,661.4305 \pm 0.0009$ (inferior conjunction of the companion star in heliocentric Julian dates) and $P = 0.21161 \pm 0.00034$ days. The above values are entirely consistent with those of FMH: $\gamma = 9.2 \pm 3.3\,{\rm km\,s^{-1}}$, $K_{\rm c} = 380.6 \pm 6.5\,{\rm km\,s^{-1}}$, and $P = 0.21159 \pm 0.00057$ days. Note that the HJDs listed in Table 1 of FMH are actually JDs; also, the phase convention of FMH differs from that adopted here.

Table 3. Radial velocity curves

Star	Spectral type	γ (km s^{-1})	$K_{\rm c}$ (km s^{-1})	χ^2 (N=17)
BD +21°652	K7 V	21 ± 8	366 ± 10	38
BD +52°857	M0 V	3 ± 8	370 ± 10	41
BD +42°2296	M0 V	-1 ± 8	365 ± 10	32
BD +44°2051	M2 V	11 ± 8	372 ± 10	41

4. Rotational broadening of the companion star

A method is used which deduces three parameters, namely, the spectral type, the rotational broadening $v \sin i$ and the fractional contribution f of the companion star to the total flux ($1 - f$ is the "veiling factor"), simultaneously (see Sect. 5 in HHF, and references therein). This is achieved by minimizing (using the χ^2 statistic) the residuals after subtracting simulated template spectra from the Doppler-corrected average spectrum. We follow exactly the same steps as in the case of Nova Oph 1977 (HSHF) and HHF. The method is illustrated in the next section. In detail, the steps of the analysis are as follows. We first deredden the object spectra (E(B-V) = 0.3 ± 0.1 mag, the average of estimates from Shrader et al. 1994 and Harlaftis & Charles 1994). The template spectra were corrected for their radial velocities and then the continua were divided by a low-order spline fit, rejecting all data above 3σ and below 1.5σ which ensured that the fits passed close to the continuum and were not biased by the numerous absorption lines and TiO bands. The object continua were normalized using a similar fit applied to the average GRO J0422+32 continuum (which has a S/N ratio $\sim$ 4 times better than the individual spectra); the latter was subsequently scaled to match each separate spectrum.

We shifted each template star to the radial velocity of each object spectrum by the amount computed from the M2 orbital solution (see Table 1). All spectra were interpolated onto

a logarithmic wavelength scale (pixel size 31.1 km s^{-1}) using a ($\sin x/x$) interpolation scheme to minimize data smoothing (Stover et al. 1980). In this way, we rebin the high signal-to-noise template spectra rather than the noisy GRO J0422+32 spectra and minimize any effect of our treatment of the data (i.e smoothing) on the results. The line broadening function affecting the object spectra consists of the convolution of the instrumental profile (FWHM = 108 km s^{-1}) with the rotational broadening profile of the companion star, with further smearing due to changes in the orbital velocity of the companion star during a given exposure. The exposure time for each object spectrum ($T_{\rm exp}$ $\approx$ 30–40 min) resulted in orbital smearing of the lines up to $2\pi K_{\rm c} T_{\rm exp}/P$, which varies between 20 and 265 km s^{-1} (see Table 1); hence, the template spectra were subsequently smeared by the amount corresponding to the orbital motion, through convolution with a rectangular profile. The resulting spectra were further broadened from 2 to 150 km s^{-1}, in steps of 10 km s $^{-1}$ (i.e., 16 steps), by convolution with the Gray (1976) rotational profile. A series of limb darkening coefficients in the range 0.4–0.7 was used to check for any differences in the results. We did not detect any change and we adopt a value of 0.5. Other effects such as the gravity darkening coefficient and the Roche-lobe geometry are not important since statistical noise is dominant (see also Sect. 5 in HHF). Next, the simulated template spectra were multiplied by a factor $0 < f < 1$ to match the absorption-line strengths of the object spectrum. Finally, we subtracted the processed template spectrum (i.e., shifted, smeared, and broadened) from the object spectrum. The residual spectrum has the spectral features of the system after subtraction of the main-sequence star (e.g., disk lines and anomalous line strengths in the companion star; see next section). The values of $\upsilon \sin i$ and f are optimized by minimizing χ^2 for each object spectrum and spectral type. The χ^2 is estimated between the residual spectrum and its smoothed version produced by Gaussian smoothing of FWHM = 933 km s^{-1} (i.e., 30 pixels). We then sum up the derived χ^2 values for each of the 21 orbital phases and each spectral type. The minimum χ^2(sum) determines the companion star's spectral type, $\upsilon \sin i$, and f.

The total χ^2(sum) for each spectral type is given in Table 4; this represents the sum of the $\chi^2_{\rm min}$ for 21 spectra (1037 degrees of freedom for each spectrum). The minimum χ^2(sum) occurs at spectral type M2 (and slightly refining the Casares et al. 1995a classification from M2$^{+2}_{-2}$ to M2$^{+2}_{-1}$). The f values (21) extracted from the M2 V template star show ellipsoidal variation which is fitted with a semi-amplitude sinusoid of 0.07 ± 0.07, consistent with (but worse than) the fit to the continuum in Fig. 2. A fit of a straight line gives $f = 0.61 \pm 0.04$; the accretion disk therefore contributes $\approx$ 40% of the light at red wavelengths. This refines the estimate of FMH of 30–60% and that of Chevalier and Ilovaisky (1995) who found a $\sim$40% contribution assuming a power-law index of 2 for the optical continuum.

Finally, against the rotational broadening of the secondary star, we added all 21 values of χ^2 for each trial rotational broadening in the range 2-150 km s^{-1} [16 groups of ($\chi^2, f, \upsilon \sin i$) for each of 21 orbital phases], using the M2 template. The resulting χ^2(sum) distribution versus $\upsilon \sin i$ has a minimum at $\upsilon \sin i = 100^{+24}_{-18}$ km s^{-1} ($\chi^2_{\rm min} + 1$ or 68% confidence level; Lampton, Margon, & Bowyer 1976). The above result is mainly driven from the five spectra with minimum smearing (smearing $\leq$ 60 km s^{-1}; see Table 1). Indeed, $\upsilon \sin i = 90^{+22}_{-27}$ km s^{-1} for spectra 2, 6, 12, 17, 19 from Table 1.

Table 4. Optimal subtraction of companion star

Star	Spectral type	f $(N = 21)$[a]	χ^2(sum)
BD +21°652	K7 V	0.47 ± 4	24191
BD +52°857	M0 V	0.57 ± 5	24143
BD +42°2296	M0 V	0.59 ± 4	24153
BD +44°2051	M2 V	0.61 ± 4	24082

[a] Fraction of the light that is contributed by the companion star at 6250 Å.

The χ^2 convergence is more difficult in GRO J0422+32 than, for example, in GS 2000+25 (HHF) because the radial-velocity smearing during a 30–40 min exposure is larger due to the shorter (5.1 hr) orbital period. (On the other hand, this is partially compensated by a smaller $K_{\rm c}$.) The disk contribution is also much larger (39 ± 3% compared to 6 ± 5%), which dilutes the photospheric lines of the companion star and makes them more difficult to detect. Finally, the S/N ratio of the individual spectra (~ 4) is poorer in GRO J0422+32 (S/N ≈ 6 for the GS 2000+25 spectra). Hence, our positive result in measuring the $\upsilon \sin i$ in the companion of GRO J0422+32 shows that the adopted technique for finding $\upsilon \sin i$ is better than the ones previously used.

We tested the above result by applying a given $\upsilon \sin i$ to a template spectrum and then attempting to recover it from simulated spectra. In detail, we apply the radial velocities of the orbital solution, smear the line profiles by the values given in Table 1, and rotationally broaden the line profiles by 50 km s^{-1}. We then apply the noise content of the observed spectra and the simulated template spectra result with the same signal-to-noise ratio as the observed ones. We finally apply a veiling of $f = 0.61$ to the spectra. In this way, we have simulated as close as possible template spectra with a given $\upsilon \sin i$ to the observed spectra. We now repeat the steps to deduce the parameters $\upsilon \sin i$, and f and find that $\upsilon \sin i = 65 \pm 19$ km s^{-1} from all 21 spectra and $\upsilon \sin i = 50^{+20}_{-50}$ km s^{-1} from the 5 spectra with smearing of $<$ 60 km s^{-1}. Clearly, $\upsilon \sin i$ is recovered from the 5 spectra alone. Inclusion of all spectra also recovers $\upsilon \sin i$ within 1σ. The uncertainty is reduced but the actual value has a systematic effect added caused by the inclusion of spectra with large smearing. Similar simulations show that use of radial velocities from the cross correlation (rather than the orbital solution) and application of zero veiling have an increasingly larger systematic effect from the expected value of $\upsilon \sin i = 50$ km s^{-1}. The above indicate that the correct $\upsilon \sin i$ can be deduced from the spectra with minimal smearing or alternatively from all the spectra within 1σ. Hence, errors in the orbital solution and veiling factor cause systematic effects and overestimate the rotational broadening. For the rest of the paper, we adopt $\upsilon \sin i = 90^{+22}_{-27}$ km s^{-1} for GRO J0422+32.

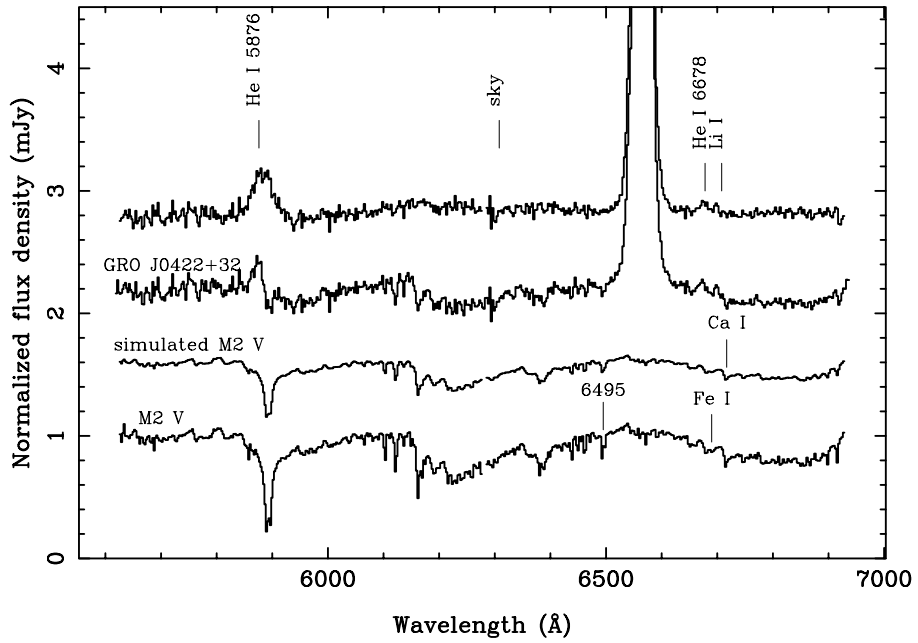

Fig. 3. Results of the technique followed to extract $v \sin i$ and f of the companion star. From bottom to top: the M2 V template BD $+44^\circ 2051$, the M2 V template convolved with a complex profile to simulate effects of orbital smearing and rotational broadening ($v \sin i = 50\,\mathrm{km\,s^{-1}}$), the Doppler-shifted average spectrum of GRO J0422+32, and the residual spectrum of GRO J0422+32 after subtraction of the companion star times $f = 0.61$. The spectra are binned to $124\,\mathrm{km\,s^{-1}}$ pixels. An offset of 0.6 mJy was added to each successive spectrum for clarity. The residual spectrum is dominated by the disk spectrum (e.g., broad Hα and He I lines in emission). Several other lines are also marked, such as the characteristic Fe I+Ca I blend at 6495 Å in G–K stars, as well as the Ca I 6717 Å and Fe I lines surrounding the absent Li I line at 6707.8 Å.

5. The M2 V subtracted spectrum

Fig. 3 summarizes the procedure we followed in the previous section, with the difference that here we use the Doppler-corrected average spectrum of GRO J0422+32 in the rest frame of the template star. The spectrum of the M2 V template (BD $+44^\circ 2051$) is shown at the bottom, binned to $124\,\mathrm{km\,s^{-1}}$ pixels (=4 pixels and similar to the instrumental resolution). This template was then treated so that its line profiles simulate those of the GRO J0422+32 spectra. The smearing velocities from Table 1 (orbital broadening) were applied to individual copies of the M2 template, and these were subsequently averaged using weights identical to those corresponding to the GRO J0422+32 spectra. Next, a rotational broadening profile corresponding to $v \sin i = 50\,\mathrm{km\,s^{-1}}$ was applied; the result is the second spectrum from the bottom in Fig. 3. The spectrum above it is the Doppler-corrected average of the GRO J0422+32 data in the rest frame of the M2 V template. Finally, the residual spectrum is shown at the top after 0.61 times the simulated M2 V template ($f = 0.61 \pm 0.04$ for M2; Table 4) was subtracted from the Doppler-shifted average spectrum.

The M-star absorption lines and TiO bands are evident in the Doppler-corrected average, and they are almost completely removed by subtraction of the template spectrum (e.g., the Na I D line). Emission from He I λ5876 becomes prominent after subtraction of the M2 V template and weak emission from He I λ6678 is also present. Note that there is no evidence for Li I λ6708 absorption, to an EW upper limit of 0.13 Å (1σ) relative to the original continuum.

6. The Hα Doppler map

We reconstruct the Doppler image of Hα using the set of spectra from January (Fig. 4), when reasonably complete orbital coverage is available. (The November data have many temporal gaps which, combined with the low S/N ratio and limited number of spectra, produce a Doppler image dominated by artifacts.) The trailed spectra are shown at the top panel which we then use to construct the Doppler maps with the maximum entropy method (MEM; Marsh & Horne 1988), a technique that has seen extensive applications in interactive binaries (e.g., Steeghs, Harlaftis, & Horne 1997; Harlaftis & Marsh 1996). The orbital phases were determined from the ephemeris given in Sect. 3. As mentioned in Sect. 4, the long exposures ($T_{\rm exp} \approx$ 30–40 min) resulted in orbital smearing of the lines up to $2\pi K_{\rm c} T_{\rm exp}/P$, which varies from 20 to $265\,\mathrm{km\,s^{-1}}$ (see Table 1). We attempted to account for the long exposure length by dividing each exposure into 6 uniformly spaced parts (using the trapezoidal rule to refine the grid). Structure in the maximum entropy images was built after successive iterations until an optimized χ^2_ν minimum was reached. The initial default image was a flat constant. After each MEM iteration, the resulting image was smoothed with a Gaussian of FWHM = $620\,\mathrm{km\,s^{-1}}$ (20 pixels) to provide the new default image. The final Doppler image was then used to build the predicted spectra by projecting the image at the observed binary phases (see bottom panels in Fig. 4 for computed spectra).

The Doppler image shows the typical ring-like distribution of an accretion disk (which projects to form the double-peaked line profiles) with emission present at velocities ranging between 300 and $1000\,\mathrm{km\,s^{-1}}$ (center panel of Fig. 4). The image is slightly shifted in the $-V_{\rm x}$ direction by $\sim$50 $\mathrm{km\,s^{-1}}$ with respect to its center on the compact object. There is no evidence for bright spot emission. Artifacts due to the sparse phase-sampling of the data (only 12 distinct phases) become evident as symmetrical rings ("Gaussian" default image). However, radial structure is not affected (see also Marsh & Horne 1988). The Hα image has a radial dependence of $V_R^{-2.7\pm0.2}$ in the range 600–$1000\,\mathrm{km\,s^{-1}}$, which corresponds to $R^{-1.65\pm0.10}$ for a Keplerian

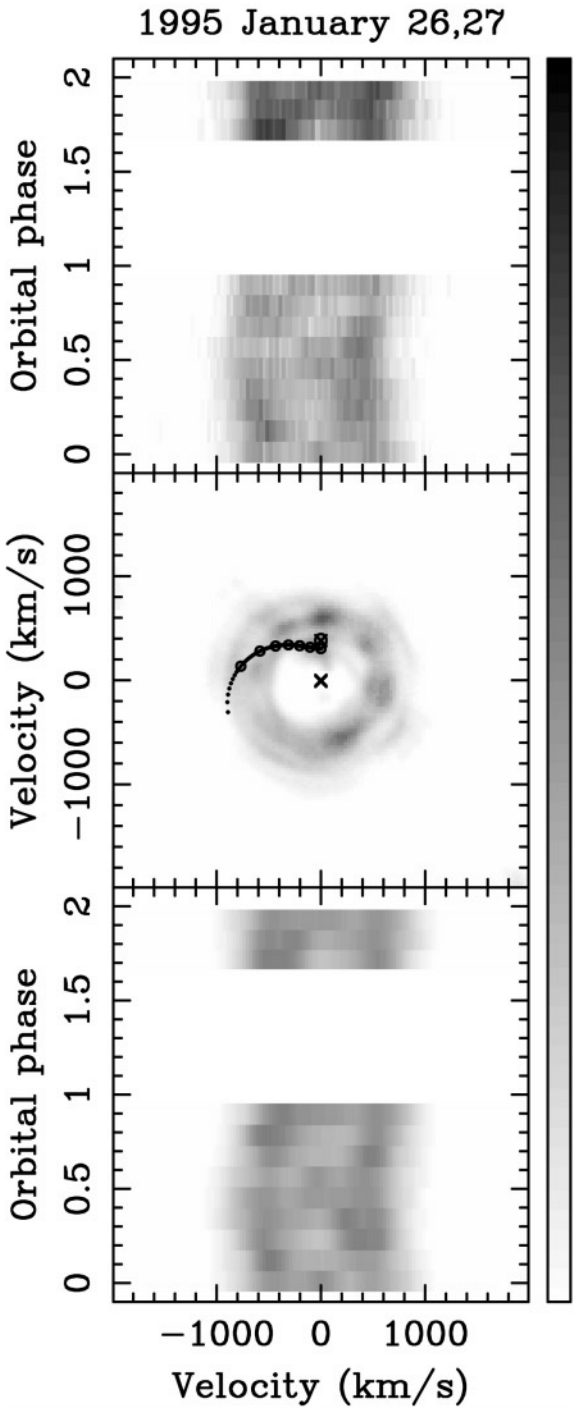

Fig. 4. Trailed spectra of Hα in 1995 January (*top panel*). The lower group is from January 26 and the upper group is from January 27. The ordinate is orbital phase, while the abscissa is velocity relative to the line center. A double-peaked profile is prominent. The MEM Doppler map (*middle panel*) shows a ring typical of accretion disk line distributions. The path of the gas stream is plotted ($q = 0.03$, $K_{\rm x} = 11\,{\rm km\,s^{-1}}$) for clarity. The *bottom panel* displays the computed spectra from the Doppler map for comparison with the observed spectra. The intensity scale is converted linearly to grey level in the right-hand strip.

Table 5. R^{-b} emissivity

Star	Line	b	Reference
A0620–00	Hα	1.5, 1.5, 1.0	1,2,3
Nova Mus 1991	Hα	1.50	2
GS 2000+25	Hα	2.15	4
GRO J0422+32	Hα	1.65	this paper

(1) Johnston, Kulkarni, & Oke 1989
(2) Orosz et al. 1994
(3) Marsh, Robinson, & Wood 1994
(4) Harlaftis, Horne, & Filippenko 1996.

field; see Appendix C in Marsh & Horne (1988) for the transformation. This can be compared to typical values of $R^{-1.5}$ found in cataclysmic variables (Horne & Saar 1991). Table 5 summarizes the Hα emissivity laws for black-hole binaries in quiescence, which show similar relations to dwarf novae. However, this may be misleading, given such a small sample, since the emissivity law may vary considerably even within the same object (e.g., A0620–00).

7. System parameters

A velocity semi-amplitude $K_{\rm c} = 372 \pm 10\,{\rm km\,s^{-1}}$ and a period $P = 0.21161 \pm 0.00034$ days imply a mass function

$$f(M_{\rm x}) = (1.13 \pm 0.09)\ M_\odot = M_{\rm x}\,\frac{\sin^3 i}{(1+q)^2},$$

consistent with the FMH estimate of $1.21 \pm 0.06\ M_\odot$. We adopt our new value because it is based on a more detailed error analysis than that of FMH. We derive the mass ratio $q = 0.116^{+0.079}_{-0.071}$ from the relation

$$\frac{v \sin i}{K_{\rm c}} = 0.462\left[(1+q)^2\,q\right]^{1/3},$$

using $v \sin i = 90^{+22}_{-27}\,{\rm km\,s^{-1}}$ (1σ). This formula is derived by assuming that the spin period of the companion star is locked to the binary period and by using Paczyński's (1971) relation for $R_{\rm c}/a$ and $q \ll 1$. Note how the mass ratio we estimate compares to the mass ratio $q = 0.109 \pm 0.009$ determined from the radial-velocity curve of the Hα profile wings ($K_{\rm H\alpha} = 42 \pm 3\,{\rm km\,s^{-1}}$; FMH). The mass ratio implies $K_{\rm x} = 43^{+29}_{-26}\,{\rm km\,s^{-1}}$. The resulting mass of the compact object is

$$M_{\rm x} = (1.4 \pm 0.2)\ \sin^{-3} i\ M_\odot,$$

while that of the companion star is

$$M_{\rm c} = (0.16^{+0.22}_{-0.15})\ \sin^{-3} i\ M_\odot.$$

To derive the actual masses, we need to know the inclination of the system. Assuming an M2 V mass of $0.39\ M_\odot$ for the companion star (Allen 1976), an inclination of $i = 48$ degrees is deduced. This, however, should be treated as a lower limit since the companion star is probably undermassive for its spectral type; see, for example, the undermassive companion stars found in A0620–00 (Marsh, Robinson, & Wood 1994)

and GS 2000+25 (HHF). The width of the Hα profile is also dependent on the inclination, if it is produced in an accretion disk ($\propto \sin\, i$; Horne & Marsh 1986). In GS 2000+25, the separation of the Hα double peaks is 1390 ± 70 km s^{-1} and most probably corresponds to an inclination of $i = 62 \pm 5^\circ$ (HHF). Scaling the peak separation of 1000 ± 70 km s^{-1} in GRO J0422+32 (and assuming similar disk radii and $M_{\rm x}$), we obtain an inclination of $i \approx 40^\circ$.

The above crude estimates are consistent with the inclinations, derived from I-band ellipsoidal variations, of $i = 41 \pm 6^\circ$ found by Casares et al. (1995a; for $q \leq 0.1$) and $i \leq 45^\circ$ found by Callanan et al. (1996b). Remodelling of the above fittings, by taking into account the 39% disk contribution in the red, would increase the derived values. The inclination is determined better by modelling the ellipsoidal modulations of the companion star from infrared photometry where the disc contribution is much lower than in the optical. However, *H*- and *K*-band photometry, surprisingly, showed no such modulation, placing only an upper limit of $i \sim 47^\circ$ (Beekman et al. 1997). Given the above uncertainties on the inclination, we use in the following a $i = 41^\circ$ as an indicative value. Evidently, infrared observations from a 10m-size telescope are required to constrain better the inclination.

The distance to GRO J0422+32 can be derived using the revised Barnes-Evans relation (Eaton & Poe 1984; Barnes & Evans 1976). Adopting Eqs. (5a) and (7) from Eaton & Poe,

$$5 \log \theta \;=\; 3.19 \;+\; 3.55\,(V-R)_0 - V_0,$$
$$0.67 < (V-R)_0 < 1.65,$$

we find

$$\log \theta = 1.605 - V/5,$$

where θ is the angular diameter of the companion star (milliarcsec) and V_0 is the dereddened apparent magnitude. We use $(V-R)_0 = 1.1$ mag for an M2 V star (Wade & Horne 1988), $E(B-V) = 0.3 \pm 0.1$ mag, and $A_V/E(B-V) = 3.1$ (Rieke & Lebofsky 1985) to derive this result. We estimate $V = 22.83 \pm 0.26$ mag for the apparent magnitude of the companion star, from $E(V-R) = 0.78\,E(B-V) = 0.23 \pm 0.08$ mag (Savage & Mathis 1979), $(V-R)_0 = 1.1$ mag for an M2 V star, $R = 20.97 \pm 0.10$ mag (Casares et al. 1995a), and a 61 ± 4% contribution of the M2 V star in R. The above relation, with $V = 22.83 \pm 0.26$ mag, then gives $\theta = (1.08 \pm 0.06) \times 10^{-3}$ milliarcsec. Finally, the distance is given by

$$d({\rm pc}) \;=\; \frac{0.462\; q^{1/3}(1+q)^{2/3} K_{\rm c}\; P}{2\pi\theta \sin i} = \frac{(v \sin i)\; P}{2\pi\theta \sin i}$$
$$=\; 2.5 \pm 0.8\ {\rm kpc},$$

using the mass-ratio formula for $R_{\rm c}/a$ of the companion star and substituting $v \sin i = 90^{+22}_{-27}$ km s^{-1}, $P = 0.21161 \pm 0.00034$ days, and $i = 41 \pm 6^\circ$. (In this relation, θ is measured in radians, not milliarcsec.) The distance uncertainty is dominated by, and scales linearly with, that in $v \sin i$. Chevalier & Ilovaisky (1995) find $d \approx 2$ kpc based on an estimate of the dereddened V magnitude of the companion star.

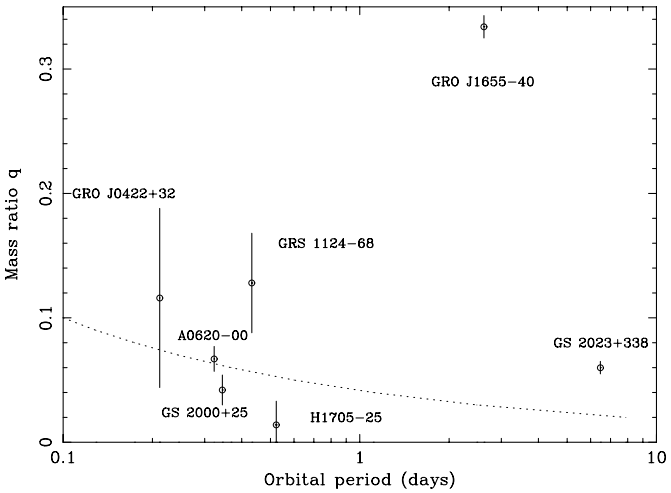

Fig. 5. The observed mass ratio (q) versus orbital period (P) for black-hole X-ray transients. The theoretical relation (q,P) conserving mass and angular momentum is also marked (*dots*), for illustrative purposes.

8. Discussion

We have reanalyzed Keck observations of GRO J0422+32 with the purpose of extending the work done by FMH. The rotational broadening, $v \sin i = 90^{+22}_{-27}$ km s^{-1}, gives a mass ratio $q = 0.116^{+0.079}_{-0.071}$ (1σ). In conjunction with the mass function of $f(M_{\rm x}) = 1.13 \pm 0.09\ M_\odot$, the mass ratio gives $M_{\rm x} = (1.4 \pm 0.2)\ \sin^{-3} i\, M_\odot$, or $M_{\rm x} \sim 5\, M_\odot$ for $i = 41^\circ$. The M2$^{+2}_{-1}$ companion star of GRO J0422+32 contributes 61 ± 4% of the light at red wavelengths (refining similar results in FMH) and derive a mass of $M_{\rm c} = (0.16^{+0.22}_{-0.15})\ \sin^{-3} i\ M_\odot$. Interestingly, we do not detect the Li I λ6708 line (EW < 0.13 Å; 1σ) in the Doppler-shifted average spectrum of GRO J0422+32. The absence of Li I in GRO J0422+32 suggests that not all low-mass X-ray binaries with K-M companion stars have high lithium abundances (see also absence of lithium in Nova Oph 1977; HSHF). It is not clear which is the source of this probably selective lithium abundance detected in five (V404 Cyg, A0620-00, GS 2000+25, Nova Mus 1991, Cen X-4) and not detected in another two soft X-ray binaries. Spallation in the inner disk during X-ray outbursts (Martín et al. 1994), spallation in an advection-dominated accretion flow (Yi and Narayan 1997) and some mechanism related to the internal structure of the companion star (HSHF) have been proposed. Convection, for example, is more important in M stars than in K stars. Moreover, recent work suggests that fast rotation may inhibit depletion of Li in stars (Martín and Claret 1996).

There are a handful of measured mass ratios in black-hole X-ray transients so far [0.067 ± 0.010 in A0620–00 (Marsh et al. 1994); 0.060 ± 0.005 in GS 2023+338 (V404 Cyg; Casares & Charles 1994); 0.042 ± 0.012 in GS 2000+25 (HHF); 0.334 ± 0.009 in GRO J1655–40 (Orosz & Bailyn 1997); $0.128^{0.044}_{0.039}$ in GRS 1124-68 (Nova Mus 1991; Casares et al. 1997); $0.014^{+0.019}_{-0.012}$ in H1705-25 (Nova Oph 1977; HSHF 1997)] which are plotted in Fig. 5. For illustrative purposes, we also plot

the relationship between P and q for conservation of mass and angular momentum,

$$P \propto \frac{(1+q)^6}{q^3},$$

which shows an increase in orbital period for mass transfer from a low-mass to a high-mass star. Such a relationship is not expected in X-ray binaries which either evolve on nuclear timescales (V404 Cyg; King 1993) or through magnetic braking (Shafter 1992). However, the mass ratio is a new observable parameter which may offer a way to test evolutionary models of low-mass X-ray binaries in the future.

Acknowledgements. The W. M. Keck Observatory, made possible by the W. M. Keck Foundation, is operated as a scientific partnership between the California Institute of Technology and the University of California. We thank L. C. Ho and T. Matheson for assistance with the observations, the Keck staff for their general support, and an anonymous referee for his useful comments. The data analysis was carried out at the STARLINK network (St. Andrews node, UK). Use of MOLLY, an interactive binary analysis package developed largely by T. Marsh, is acknowledged. This research has benefitted from the SIMBAD data base, operated at CDS, Strasbourg, France. AVF is grateful for support through NSF grant AST–9417213, as well as for an appointment as a Miller Research Professor in the Miller Institute for Basic Research in Science (UC Berkeley).

References

Allen C.W., 1976, Astrophysical Quantities. 3d ed., Athlone, London
Barnes T.G., Evans D.S. 1976, MNRAS 174, 489
Beekman G., Shahbaz T., Naylor T., Charles P.A., 1996, MNRAS 281, L1
Callanan P.J., Garcia M.R., Filippenko A.V., McLean I., Teplitz, H., 1996a, ApJ 470, L57
Callanan P.J., Garcia M.R., McClintock J.E., Zhao P., 1996b, ApJ 461, 351
Casares J., Charles P.A., 1994, MNRAS 271, L5
Casares J., Charles P.A., Marsh T.R., 1995, MNRAS 277, L45
Casares J., Charles P.A., Naylor T., 1991, Nat 355, 614
Casares J., Martin A.C., Charles P.A., et al., 1995a, MNRAS 276, L35
Casares J., Marsh T.R., Charles P.A., et al., 1995b, MNRAS 274, 565
Casares J., Martín E.L., Charles P.A., Molaro P., Rebolo R., 1997, New Astronomy 1, 299
Chevalier C., Ilovaisky S.A., 1995, A&A 297, 103
Eaton J.A., Poe C.H., 1984, Acta Astron. 34, 97
Filippenko A.V., Matheson T., Barth A.J., 1995, ApJ 455, L139 (FMB)
Filippenko A.V., Matheson T., Ho L.C., 1995, ApJ 455, 614 (FMH)
Garcia M.R., Callanan P.J., McClintock J.E., Zhao P., 1996, ApJ 460, 932
Gray D.F., 1976, The Observations and Analysis of Stellar Photospheres. Wiley-Interscience, New York, 373
Harlaftis E.T., Charles P.A., 1994, IAU Circ. No. 5728
Harlaftis E.T., Horne K., Filippenko A.V., 1996, PASP 108, 762 (HHF)
Harlaftis E.T., Marsh T.R., 1996, A&A 308, 97
Harlaftis E.T., Steeghs D., Horne K., Filippenko A.V., 1997, AJ 114, 1170
Haswell C.A., 1995, In: van Paradijs J., van den Heuvel E.P.J., Kuulkers E. (eds.) Compact Objects in Close Binaries. IAU Symp. 165, Kluwer, Dordrecht, 351
Horne K., 1986, PASP 98, 609
Horne K., Marsh T.R., 1986, MNRAS 218, 761
Horne K., Saar S.H., 1991, ApJ 374, L55
Johnston H.M., Kulkarni S.R., Oke J.B., 1989, ApJ 345, 492
King A.R., 1993, MNRAS 260, L5
Lampton M., Margon B., Bowyer S., 1976, ApJ 208, 177
Marsh T.R., Horne K., 1988, MNRAS 235, 269
Marsh T.R., Robinson E.L., Wood J.H., 1994, MNRAS 266, 137
Martín E.L., Rebolo R., Casares J., Charles P.A., 1994, ApJ 435, 791
Martín E.L., Claret A., 1996, A&A 306, 408
Oke J.B., et al., 1995, PASP 107, 375
Orosz J.A., Bailyn C.D., Remillard R.A., McClintock J.E., Foltz C.B., 1994, ApJ 436, 848
Orosz J.A., Bailyn C.D., 1995, ApJ 446, L59
Orosz J.A., Bailyn C.D., 1997, ApJ 477, 876
Paczyński B., 1971, ARA&A 9, 183
Remillard R.A., Orosz J.A., McClintock J.E., Bailyn C.D., 1996, ApJ 459, 226
Rieke G.H., Lebofsky M.J., 1985, ApJ 288, 618
Savage B.D., Mathis J.S., 1979, ARA&A 17, 73
Shafter A.W., 1992, ApJ 394, 268
Shrader C.R., Wagner R.M., Hjellming R.M., Han X.H., Starrfield S.G., 1994, ApJ 434, 698
Steeghs D., Harlaftis E.T., Horne K., 1997, MNRAS 290, L28
Stover R.J., Robinson E.L., Nather R.E., Montemayer T.J., 1980, ApJ 240, 597
van Paradijs J., McClintock J.E., 1995, In: Lewin W.H.G., van Paradijs J., van den Heuvel E.P.J. (eds.) X-Ray Binaries. Cambridge Univ. Press, Cambridge, 107
Wade R.A., Horne K., 1988, ApJ 324, 411
Welsh W.F., Horne K., Gomer R., 1995, MNRAS 275, 649
Yi I., Narayan R., 1997, ApJ 486, 363